LBL-11124

Lawrence Berkeley Laboratory
UNIVERSITY OF CALIFORNIA

Materials & Molecular Research Division

GAS-SOLID INTERFACE REACTION

Mei Chang
(M.S. thesis)

July 1980

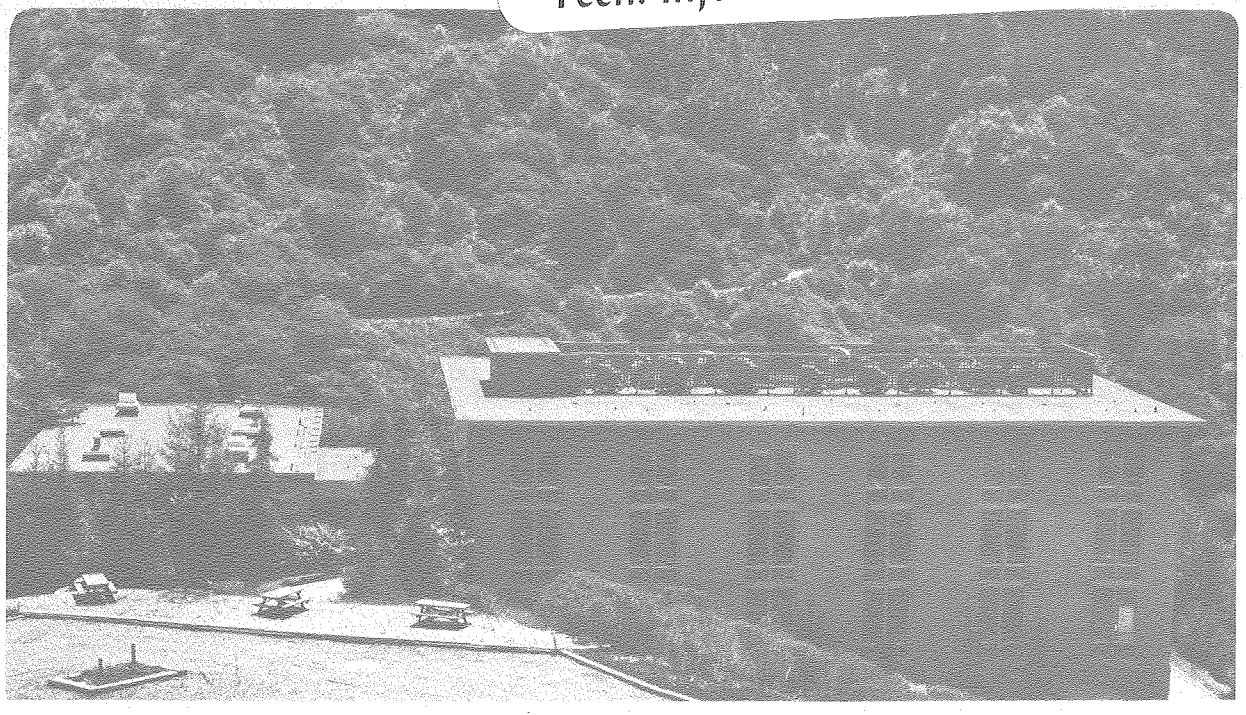

Prepared for the U.S. Department of Energy under Contract W-7405-ENG-48

DISCLAIMER

LBL-11124

GAS-SOLID INTERFACE REACTION

Mei Chang

Materials and Molecular Research Division
Lawrence Berkeley Laboratory
and
Department of Materials Science and Mineral Engineering
University of California
Berkeley, California 94720

This work was supported by the U.S. Department of Energy
under contract No. W-7405-ENG-48.

TABLE OF CONTENTS

TABLE OF CONTENTS (continued)

GAS-SOLID INTERFACE REACTION

Mei Chang

Materials and Molecular Research Division
Lawrence Berkeley Laboratory
and
Department of Materials Science and Mineral Engineering
University of California
Berkeley, California 94720

ABSTRACT

The reduction kinetics of dense $CoFe_2O_4$ by pure hydrogen were studied thermogravimetrically in the temperature range of 560°C to 620°C, and in the pressure range of 50 torr to 250 torr. Under these experimental conditions, a porous topochemical metal product layer formed, with a simple oxide/metal interface. The reduction reaction was found to be under mixed control. The contribution of the gas diffusion resistance and of the interface reaction resistance were determined using a mathematical model based on one derived by Spitzer, Manning and Philbrook. It was found that the effective gas diffusion coefficient depended weakly on temperature, while the interface reaction followed Langmuir-Hinshelwood kinetics.

The nature of the rate controlling steps in the interface reaction could be deduced from the form of the interface reaction rate expression and from the activation energies of certain reaction rate parameters. Both a surface chemical reaction and an interface diffusion of excess cations were found to be involved.

The morphology of the reduced product layer was examined by scanning electron microscopy. The pore structure was composed of macropores (or intergranular pores) and micropores (or intragranular pores). The pore size depended on the reaction temperature, but not on the pressure. At lower temperatures the macropores were larger and the micropores were small. With increasing temperatures, the scale pore structure became more uniform and tended towards a larger average pore size. The scale, however, appeared not to densify; only pore coarsening occurred. The gas diffusion was mainly through the macropore at 580^{o}C, but was increasingly shaped by the micropores towards 620^{o}C.

NOTATIONS

A_1, A_2	Experimental constant in the interface reaction rate equation 3.1
C_i	Concentration of species i
C_i^b	Concentration of species i in the bulk stream
C_i^i	Concentration of species i at the reaction interface
C_i^o	Concentration of species i at the specimen surface
c_o	Concentration of oxygen in oxide
D	Gas diffusion coefficient
D_a	Gas diffusion coefficient in macropores
D_i	Gas diffusion coefficient in micropores
D_{eff}	Effective gas diffusion coefficient
D_{effi}	Effective gas diffusion coefficient of species i
D_{ij}	Binary gas diffusion coefficient of species i and j
D_K	Knudsen diffusion coefficient
D_{Ka}	Knudsen diffusion coefficient in macropores
D_{Ki}	Knudsen diffusion coefficient in micropores
D_s	Interface diffusion coefficient
D_v	Volume diffusion coefficient
J	Flux of reaction species
k	Experimental constant defined in equation 3.4
k'	Rate constant in equation 1.6
k_1	Forward reaction rate constant of hydrogen adsorption
k_{-1}	Reversed reaction rate constant of hydrogen adsorption

k_2	Forward reaction rate constant of modified surface reaction
k_{-2}	Reversed reaction rate constant of modified surface reaction
k_2'	Forward reaction rate constant of surface reaction
k_{-2}'	Reversed reaction rate constant of surface reaction
k_3	Reversed reaction rate constant of water desorption
k_{-3}	Forward reaction rate constant of water desorption
k_4	Diffusion rate constant of excess cation to metal sink
k_m	External mass transfer coefficient
k_{mi}	External mass transfer coefficient of species i
k_{ov}	Rate constant in Spitzer's model (equation 1.7)
k_r	Interface reaction rate constant
K_1	Equilibrium constant of hydrogen adsorption
K_2	Equilibrium constant of modified surface reaction
K_2'	Equilibrium constant of surface reaction
K_3	Equilibrium constant of water adsorption
K_e	Overall equilibrium constant
L	Characteristic diameter of specimen
M_i	Molecular weight of species i
p_i	Pressure of species i
p_i^b	Pressure of species i in the bulk stream
R	Reaction rate
R_1	Reaction rate of hydrogen adsorption
R_2	Reaction rate of surface reaction

R_3	Reaction rate of water desorption
R_4	Solid state diffusion rate
R_g	Gas constant
r_o	Radius of sphere
r	Radius of unreacted core
r_a	Size of macropore
r_i	Size of micropore
t	Time
T	Temperature
u	Interface advancing rate
X	Fractional extent of reaction
ε	Porosity
ε_a	Volume fraction of macropores
ε_i	Volume fraction of micropores
θ_i	Fraction of surface sites occupied by species i
θ_S	Fraction of vacant surface sites
$\theta_{i/M}$	Fraction of excess metal surface sites occupied by species i
$\theta_{i/OM}$	Fraction of oxide surface sites occupied by species i
λ	Average source to sink distance for solid state diffusion
μ	Viscosity
ξ	Metal layer thickness
ρ	Density

1. INTRODUCTION

Gas-solid reactions are frequently encountered in industry, for example in the reduction of oxides, in the decomposition of carbonates, and in high temperature corrosion of metals. The reduction reactions occurs in five distinct steps:

(1) External mass transfer of the reactant gas

(2) Diffusion of the reactant gas through the dense and/or porous solid products

(3) Chemical reaction at the interface

(4) Diffusion of the product gas through the dense and/or porous solid products

(5) External mass transfer of the product gas.

The transport of reactant gas from the bulk stream to the outer surface of specimen is the external mass transfer process. The gas velocity near the specimen surface is slowed down by the friction between gas and solid. This gives rise to a film, called the "boundary layer", surrounding the specimen. The partial pressure of the reactant gas at the solid surface may therefore be lower than in the bulk stream. For the product gas, the reverse would be true.

Further, reaction is hindered by the solid product layer. If the product layer is porous, gas can diffuse easily through the layer to reach the reaction interface. If the product layer is dense, solid state diffusion will play a very important role. In the present work on reduction of a mixed oxide spinel-cobalt

ferrite by hydrogen, a porous metal layer was produced. Thus, only gas phase diffusion was considered.

The interface chemical reaction is not a simple step. It depends on local parameters such as the interface gas concentration and the composition of the solid. A lot of substeps may be involved in the interface chemical reaction, including adsorption, desorption, surface dissociation and association, short range solid state diffusion of cations and anions near the reaction interface, phase transformation, and nucleation and growth phenomena. A probe of the details of the interface reaction is the purpose of this work.

1.1. Kinetics

Per unit area, the rate of gas transfer from the bulk stream to the external solid surface is given by

$$J = k_m(C^b - C^o)^* \qquad (1.1)$$

where k_m is the external mass transfer coefficient defined by equation 1.1.

Mass transfer has been studied well. A frequently used expression for a spherically shaped solid was given by Ranz and Marshall (1).

$$\frac{k_m L}{D} = 2.0 + 0.6 \left(\frac{\rho V L}{\mu}\right)^{1/2} \left(\frac{\mu}{\rho D}\right)^{1/3} \qquad (1.2)$$

---

*See Notation for the definitions of all the symbols.

where the $k_m L/D$ is defined as the Sherwood number, $\rho VL/\mu$ as the Reynolds number, and $\mu/\rho D$ as the Schmidt number. If the temperature, pressure and specimen size and shape are fixed, the external mass transfer coefficient is only related to gas velocity, V.

If the gas velocity is very low, it is possible that the external mass transfer controls the overall reaction and the reaction rate depends on the gas velocity. This "gas starvation" has been considered recently by Hills (2). At lower bulk stream velocity, the boundary layer gets thicker, and the reaction rate becomes slower.

Gas diffusion can be described by Fick's law. The diffusion rate is proportional to the concentration gradient. The proportionality constant is called the diffusion coefficient. In a porous system, the diffusion coefficient depends on the pore structure, size and connectivity. An effective diffusion coefficient, D_{eff}, is thus used to describe the gas transport. D_{eff} includes all structural effects of the porous scale. For simplicity, an average concentration gradient will be used and the diffusion equation is

$$J = D_{eff} \left(\frac{C^o - C^i}{\xi} \right) \tag{1.3}$$

If the overall reaction is controlled by this step, the product layer growth will obey a parabolic law, that is:

$$\xi = k_p \, t^{1/2} \tag{1.4}$$

where k_p is a rate constant. Here, we assumed that the effective diffusion coefficient did not depend on time. In practice, sintering may change the morphology of the product layer, and then the effective diffusion coefficient is not a constant for sufficiently large reaction times.

When the interface process is rate limiting, the reaction rate will not depend on the product layer thickness, and linear layer growth kinetics must be observed for a flat, semi-infinite solid.

1.2. Oxide reduction model

Much modeling work has been done from an engineering viewpoint. The parametric relationship between the extent of reaction and the time for different geometries is then determined. McKewan (3) proposed a simple rate equation for a reduction reaction limited by the interface process. For a dense spherical or cube-shaped specimen, he found:

$$1 - (1 - X)^{1/3} = k' t \qquad (1.5)$$

or

$$\xi = k' t \qquad (1.6)$$

where X is extent of reaction defined as X = (wt. loss)/(total possible wt. loss). McKewan's data fit his equation quite well.

Although it is clear that exclusive interface reaction control will yield linear layer growth kinetics, Spitzer et al. (4)

demonstrated that linear layer growth kinetics may also be observed when gas diffusion in the product layer plays a significant role in the overall reaction. In Spitzer et al.'s model, the resistance of all three of the components were incorporated. The equation derived for a spherically shaped solid was:

$$(1 - (1 - X)^{1/3}) = \frac{k_{ov}}{R_g T r_o c_o} \left(p_A^b - \frac{p_B^b}{K_e} \right) \tag{1.7}$$

where

$$k_{ov} = 1/\left[\frac{1}{3\alpha} \left(1 + \frac{r}{r_o} + \left(\frac{r}{r_o} \right)^2 \right) + \frac{r_o}{6\beta} \left(1 + \frac{r}{r_o} - 2\left(\frac{r}{r_o} \right)^2 \right) + \frac{1}{k_r} \right] \tag{1.8}$$

In this equation, k_r is the specific rate constant for the interface reaction. The coefficient α and β are given by

$$\alpha = \frac{K_e k_{mA} k_{mB}}{K_e k_{mB} + k_{mA}} \tag{1.9}$$

and

$$\beta = \frac{K_e D_{effA} D_{effB}}{K_e D_{effB} + D_{effA}} \tag{1.10}$$

Spitzer's model is limited to reactions having a sharp interface between the product layer shell and the unreacted core, i.e. topochemical reactions. This "shrinking core model" can be used in the reduction of dense oxides.

Turkdogan et al. (5,6,7,8) have done a thorough experimental investigation of the reduction of dense and porous iron oxide.

They developed their own model and promoted the idea that mixed interface and gas diffusion control in the early stage of the reaction will shift gradually to gas diffusion control.

A general structural model for gas-solid reaction has been developed by Szekeley et al. (9). In this model, one can easily calculate the extent of reaction as a function of time if the characteristic parameters of the system are known.

1.3. Interface reaction

The interface reaction kinetics in most of the modeling work were assumed to be first order, irreversible or reversible. Langmuir-Hinshelwood kinetics were also considered by Szekeley et al. (9), but the overall rate expression can not be formulated analytically for general geometries; it can only be solved numerically. McKewan (3) obtained Langmuir-Hinshelwood kinetics for the hydrogen-iron oxide interface reaction and interpreted it by an adsorption, surface reaction and desorption mechanism. In his analysis, the influence of gas diffusion was not considered, however.

In order to obtain reliable interface reaction kinetics, the effects of external mass transfer and gas diffusion through the product layer have to be subtracted. For geometrical simplicity, a slab of dense oxide was chosen for the present work. We followed the analysis of Spitzer's as described by Porter and De Jonghe (10). The general scheme for the reaction is sketched in Fig. 1. The flux equations for every step then are shown as follows:

(1) external mass transfer of reactant gas

$$J = k_{mH_2}\left(C^{b}_{H_2} - C^{o}_{H_2}\right) \tag{1.11}$$

(2) reactant gas diffusion in the porous product layer

$$J = \frac{D_{effH_2}}{\xi}\left(C^{o}_{H_2} - C^{i}_{H_2}\right) \tag{1.12}$$

(3) interface reaction

$$J = k_r\left(C^{i}_{H_2} - \frac{1}{K_e} C^{i}_{H_2O}\right) \tag{1.13}$$

(4) product gas diffusion in porous product layer

$$J = \frac{D_{effH_2O}}{\xi}\left(C^{i}_{H_2O} - C^{o}_{H_2O}\right) \tag{1.14}$$

(5) external mass transfer of product gas

$$J = k_{mH_2O}\left(C^{o}_{H_2O} - C^{b}_{H_2O}\right) \tag{1.15}$$

Here, we assume that the reactant gas is pure hydrogen and the product gas is water.

In the quasi steady state, the fluxes in every steps are equal. Combining the equation 1.11 to 1.15 and eliminating the intermediate concentration terms, one obtains:

$$J\left[\left(\frac{1}{k_{mH_2}}+\frac{1}{K_e k_{mH_2O}}\right)+\xi\left(\frac{1}{D_{effH_2}}+\frac{1}{K_e D_{effH_2O}}\right)+\frac{1}{k_r}\right] = C^b_{H_2}-\frac{1}{K_e}C^b_{H_2O} \tag{1.16}$$

If $K_e \gg 1$ and if the bulk gas is pure hydrogen, equation 1.16 can be further simplified to:

$$\frac{C^b_{H_2}}{J}=\left(\frac{1}{k_m}+\frac{1}{k_r}\right)+\xi\frac{1}{D_{eff}} \tag{1.17}$$

The plot of the reciprocal flux against the scale thickness, ξ, will show a straight line if the diffusion coefficient, D_{eff}, and the interface reaction rate constant, k_r, are independent of the scale thickness. Then the value of k_r can be determined unambiguously. Information about the interface reaction can thus be deduced from the temperature and pressure dependence of k_r.

1.4. Cobalt ferrite

Rey (11) has done some work on the reduction of cobalt ferrite by hydrogen. Below 500°C, a clear boundary attack was observed and some unreduced oxide was retained in the scale in the vicinity of the interface. An anomolous reaction rate drop occurs at about 650°C. This drop was related to the formation of wüstite sublayer. For the sake of consistency in the analysis, the experimental temperatures were therefore chosen within the range of 500°C to 650°C. Porter and De Jonghe (10) observed that the linear relationship

between the reciprocal flux and the scale thickness was valid below 650^{o}C and proposed an interface reaction mechanism involving solid state diffusion, such as one briefly considered by Wagner (12). Wagner, however, appeared to rule out solid state diffusion control on the basis that the interface is near equilibrium. In this work we cannot adopt this assumption.

2. EXPERIMENTAL

2.1. Apparatus

The rate of reduction of cobalt ferrite by hydrogen were measured by thermogravimetry. A sketch of the experimental system is shown in Fig. 2. The system consists of a Cahn RG thermobalance and a vertical furnace. The weighing mechanism was enclosed in a glass chamber and the specimens were suspended in a 19 mm quartz tube. The hydrogen gas passed from top to the bottom of the tube. The gas flow rate was controlled and monitored by Matheson 602 flowmeter, and the pressure of the flowing gas was held constant to within $\pm$ 0.5 torr between 25 torr and 400 torr by a downstream pressure regulator. The temperature of furnace was controlled to within $\pm$ 1^{o}C and was monitored by a K type thermocouple.

99% dense, crystalline cobalt ferrite was supplied by Countis Industries. It had grain size of about 10 μ. The hydrogen gas was provided and analyzed by Matheson Co. The water content was controlled at about 100 ppm.

2.2. Experimental procedure

The cobalt ferrite specimens were cut from the bar of raw material to a dimension of 1 cm x 1 cm x 0.06 cm, and slightly polished. The specimens were hung by a 0.127 mm chromel wire from the balance into the furnace. Then the system was evacuated to about 0.2 torr and the furnace was turned on. Once the desired temperature was reached and had stabilized, the flow of hydrogen was started. The weight of specimens was recorded continuously

after evacuation. There was no weight loss in the period of heating. After the gas flow was started, it took 30 to 60 seconds to reach the desired, steady gas pressure and the data were lost in this period. When the reaction was completed the weight did not change any more. The completely reduced specimens then were cooled in flowing hydrogen to prevent reoxidation. The final weight was checked by a conventional balance.

The rate of weight loss will depend on the hydrogen flow rate at low flow rate because of hydrogen starvation or external mass transfer resistance. The hydrogen flow rate was set at a sufficiently high rate so that the gas flow rate did not affect the behavior of reduction. In experiments, the hydrogen flow rate was set at 25 ml STP per second.

The data generated by thermogravimetric analysis were the instantaneous weight of the specimens as a function of time. Since the reaction proceeds in a topochemical fashion, without measureable macroscopic shrinkage, the thickness of reacted shell can be simply calculated from the weight loss data and the instantaneous reaction rate can be obtained.

Specimens for microstructural examination were reduced in the same experimental apparatus and under the same reaction conditions. After a short reaction time, the reactions were stopped by dropping the specimens out of the hot zone and quenching them. Polished surfaces and fractured surfaces of partially reduced specimens were examined by scanning electron microscopy and by optical microscopy. The preparation of polished specimens was

done according to the following procedure: First, the specimens were vacuum mounted in epoxy resin. Then, the mounted specimens were ground through 320, 400, and 600 grit silicon carbide paper. After ultrasonic cleaning, they were polished on nylon cloth with 1 μ alumina dispersed in distilled water. The final polishing was done with 0.05 μ alumina on microcloth for 5 minutes.

3. RESULT

3.1. Thermogravimetric analysis

The rates of metal layer growth on cobalt ferrite were measured in the temperature range of 560°C to 620°C and in the pressure range of 50 torr to 250 torr. Figure 3 shows the layer thickness, ξ, as a function of time at 200 torr of hydrogen, at the four selected temperatures: 560°C, 580°C, 600°C, and 620°C. Figure 4 shows the layer thickness, ξ, as a function of time at 580°C, at five different pressures: 50 torr, 100 torr, 150 torr, 200 torr, and 250 torr. The data in Fig. 4 show that an increase of temperature and of pressure increases the rate of metal layer growth.

From the mathematical analysis described in the previous section, it follows that if the hydrogen concentration at the reaction interface is close to that of bulk gas phase, the reciprocal of the reaction rate, $\dot{\xi}^{-1}$, will be linearly dependent on metal layer thickness, ξ. In the temperature range of 560°C to 620°C, it is indeed observed that a linear relationship is followed. Figure 5, a typical rate plot for reduction at 580°C, shows that the linear relationship is maintained up to a layer thickness of 0.25 mm. Then, the reaction kinetics can be analyzed in terms of equation 1.17. The value of $(k_m^{-1} + k_r^{-1})$ corresponds to the extrapolated reciprocal reaction rate at zero layer thickness. The effective diffusion coeficient, D_{eff}, can be calculated from the slope. The values of $(k_m^{-1} + k_r^{-1})^{-1}$ and D_{eff} have been listed in Table 1 and Table 2.

3.2. External mass transfer

The external mass transfer coefficient, k_m, can be calculated reliably from standard fluid mechanic expressions. The calculation has been given in Appendix 1. The calculated values of k_m at 600°C, with pressures of 50 torr and 250 torr are 378 cm/sec and 75 cm/sec respectively. They do not depend significantly on temperature in the range of 560°C to 620°C.

At 600°C and 250 torr, the experimental value of $(k_m^{-1} + k_r^{-1})^{-1}$, as listed in Table 2, is 4.25 cm/sec. The calculated value of k_r, under the same conditions, is 4.50 cm/sec. The difference between k_r and $(k_m^{-1} + k_r^{-1})^{-1}$ is only 5%. At 600°C and 50 torr, the difference drops to 3%. From this comparison, it is obvious that the effect of external mass transfer is very small and can be neglected. The value of $(k_m^{-1} + k_r^{-1})^{-1}$ is equivalent to that of k_r^{-1} within the experimental error.

3.3. Interface reaction

Figure 6 shows that the reciprocal interface reaction rate constant, k_r, is proportional to the hydrogen concentration in the bulk phase, $C_{H_2}^b$. Mathematically, this can be written as

$$k_r^{-1} = A_1 + A_2 C_{H_2}^b \qquad (3.1)$$

For a reversible reaction, the interface reaction equation is thus:

$$R = k_r \left(C^i_{H_2} - \frac{1}{K_e} C^i_{H_2O} \right) \tag{3.2}$$

$$= \frac{C^i_{H_2} - \frac{1}{K_e} C^i_{H_2O}}{A_1 + A_2 C^b_{H_2}} \tag{3.3}$$

If there exists a relationship between the bulk concentration and the interface concentrations such as

$$C^b_{H_2} = C^i_{H_2} + k C^i_{H_2O} \tag{3.4}$$

the rate equation will follow Langmuir-Hinshelwood kinetics.

$$R = \frac{C^i_{H_2} - \frac{1}{K_e} C^i_{H_2O}}{A_1 + A_2 C^i_{H_2} + k A_2 C^i_{H_2O}} \tag{3.5}$$

The constant k can be represented by the pressure difference between the reaction interface and the bulk phase. If there is no pressure gradient in the metal scale, the constant k will be equal to 1.

When $(1/K_e)C^i_{H2O} \ll C^i_{H_2}$, or for an irreversible reaction, the rate equation can be simplified:

$$R = \frac{C^i_{H_2}}{A_1 + A_2 C^i_{H_2} + k A_2 C^i_{H_2O}} \tag{3.6}$$

4. DISCUSSION

4.1. Gas Diffusion

There are three possible mechanisms of gas diffusion in porous media (13): (a) ordinary molecular diffusion (b) Knudsen diffusion (c) surface diffusion. Ordinary molecular diffusion results from partial pressure gradients. For a binary mixture for example, in the H_2 - H_2O system, the ordinary molecular diffusion coefficient, D_{H_2/H_2O}, is proportional to the 3/2 power of absolute temperature and to the reciprocal of the total pressure. Knudsen diffusion will prevail, if the gas density is low, or if the pores are quite small, or both, so that the molecules collide with the pore wall much more frequently than with each other. The Knudsen diffusion coefficient, D_K, is proportional to the 1/2 power of temperature and to the pore radius. Transport by surface diffusion cannot be significant unless appreciable adsorption occurs; yet if adsorbed molecules are held so strongly as to be essentially immobile, surface diffusion will again be insignificant. The value of a surface diffusion coefficient is typically in the range of 10^{-9} to 10^{-12} cm^2/sec at ambient temperature for hydrogen on metal (13). Comparing with the experimental values in Table 1, the surface diffusion contribution can be ignored.

Ordinary molecular diffusion occurs when the collision frequency of molecules with the pore wall are unimportant compared to the molecular collision frequency in the free space of the pore. Knudsen diffusion occurs when this condition is reversed. In a given pore there is a range of molecular concentrations in which

both type of collisions are important. This is the "transition" regime.

Figure 7 shows the microstructure of the metal scale. The pore structure consists of an intergranular pore network and an intragranular pore network. The size of the macropores (intergranular pores) decreases with increasing reaction temperature, but the size of the micropores (intragranular pores) increases with increasing reaction temperature. The macropore sizes were in the range of 0.2 μ to 2 μ. Appendix 2 shows that the diffusion in the macropores is in the transition region. For a H_2/H_2O mixture with equimolar counterdiffusion in the transition region, the diffusion coefficient is (14):

$$D^{-1} = D^{-1}_{H_2/H_2O} + D^{-1}_K \qquad (4.1)$$

The effective diffusion coefficient, D_{eff}, is related to the detailed pore structure. Wakao and Smith (15) proposed a "random pore" model that divides the pores into micropores and macropores and represents the diffusion flux as being the sum of that through the macropores, that through the micropores and that through both in series. The effective diffusion coefficient in this model is given by

$$D_{eff} = \left[\varepsilon_a^2 D_a + \varepsilon_i^2 D_i + 2\varepsilon_a(1-\varepsilon_a) \left(\frac{2\varepsilon_i^2}{\frac{\varepsilon_i^2}{D_a} + \frac{(1-\varepsilon_a)^2}{D_i}} \right) \right] \qquad (4.2)$$

Appendix 3 shows the comparison of calculated value and measured value. Wakao and Smith's model works quite well.

The first term in equation 4.2 represents the contribution of macropores alone, and the second term represents that of micropores alone. By examining the values in Appendix 3, we can find that the dominant contribution was from macropores at 560°C and from micropores at 620°C. This shift is the reason why the effective diffusion coefficient did not show a strong dependence on temperature and pressure in the experimental conditions.

4.2. Interface reaction

The interface reaction is schematically shown in Fig. 8. The hydrogen molecules adsorbed on the oxide surface react with oxygen to form water, produce excess cations on the surface. Then, the water molecules desorb from the surface. The excess metal cations will diffuse to the metal sink. At the same time, the oxygen anions have to diffuse out of the metal oxide interface to permit the advancing of the interface. Although the interface appears very complicated, it can be described by the following steps:

(1) adsorption

$$H_{2(g)} \underset{k_{-1}}{\overset{k_1}{\rightleftharpoons}} H_{2(ad)} \qquad (4.3)$$

(2) chemical process (oxygen exchange)

$$H_{2(ad)} + M_xO \underset{k'_{-2}}{\overset{k'_2}{\rightleftharpoons}} H_2O_{(ad)} + xM^{\cdot\cdot} + 2x\ e' \qquad (4.4)$$

(3) desorption

$$H_2O_{(ad)} \underset{k_3}{\overset{k_{-3}}{\rightleftharpoons}} H_2O_{(g)} \qquad (4.5)$$

(4) solid state diffusion near or in the interface

$$M^{\cdot\cdot} + 2\ e' \xrightarrow{k_4} M_{(sink)} \qquad (4.6)$$

The rate expression of the interface reaction can be derived from the arguments of the rate determining steps and quasi steady state assumption. The actual rate determining step then can be found by comparing the experimentally determined relationships with the various theoretical ones.

If the solid state diffusion did not control the reaction as in the case of (a), (b), and (c), the step (2) and the step (4) can be combined to

$$H_{2(ad)} + M_xO \underset{k_{-2}}{\overset{k_2}{\rightleftharpoons}} H_2O_{(ad)} + M \qquad (4.4a)$$

The analysis follows that of Szekely, Evans and Sohn (9).

(a) adsorption control

The rate equation is

$$R = R_1 = k_1 C_{H_2} \theta_S - k_{-1} \theta_{H_2} \tag{4.7}$$

Applying the quasi steady state assumption, the step (2) and step (3) are in equilibrium.

$$K_2 = \frac{k_2}{k_{-2}} = \frac{\theta_{H_2O}}{\theta_{H_2}} \tag{4.8}$$

$$K_3 = \frac{k_3}{k_{-3}} = \frac{\theta_{H_2O}}{C_{H_2O}\theta_S} \tag{4.9}$$

If the excess metal ions did not affect the adsorption, that is the metal ions produced in steps (2) did not occupy an active surface site, we have

$$\theta_S + \theta_{H_2} + \theta_{H_2O} = 1 \tag{4.10}$$

from the overall balance on the sites.

From equation 4.8, 4.9, and 4.10, the expression for θ_S and θ_{H_2} can be obtained

$$\theta_S = \frac{1}{(1 + (K_3 + K_3/K_2)\ C_{H_2O})} \tag{4.11}$$

$$\theta_{H_2} = \frac{K_3}{K_2} C_{H_2O} \theta_S \tag{4.12}$$

Substituting θ_S, θ_{H_2} into equation 4.7, the rate equation becomes

$$R = \frac{k_1 \left(C_{H_2} - \frac{1}{K_e} C_{H_2O} \right)}{1 + (K_3 + K_3/K_2) C_{H_2O}} \tag{4.13}$$

and

$$k_r^{-1} = k_1^{-1} + k_1^{-1}(K_3 + K_3/K_2) C_{H_2O} \tag{4.14}$$

where K_e is overall equilibrium constant

$$K_e = \frac{K_1 K_2}{K_3} = \frac{k_1 k_2 k_{-3}}{k_{-1} k_{-2} k_3} \tag{4.15}$$

(b) desorption control

The step (1) and step (3) are assumed in equilibrium. Using similar procedure as in (a), if the excess metal ion did not occupy an active surface site, we obtain

$$\theta_S = \frac{1}{(1 + (K_1 + K_2 K_1) C_{H_2})} \tag{4.16}$$

$$\theta_{H_2O} = K_1 K_2 C_{H_2} \theta_S \tag{4.17}$$

and

$$R = R_3 = k_{-3} \theta_{H_2O} - k_3 C_{H_2O} \theta_S \tag{4.18}$$

$$= \frac{k_3 K_e \left(C_{H_2} - \frac{1}{K_e} C_{H_2O} \right)}{1 + (K_1 + K_2 K_1) C_{H_2}} \tag{4.19}$$

$$k_r^{-1} = k_3^{-1} K_e^{-1} + k_3^{-1} K_e^{-1} (K_1 + K_2 K_1) C_{H_2} \tag{4.20}$$

(c) chemical control

In this case, under the same assumption, the rate equation becomes

$$R = R_2 = k_2 \theta_{H_2} - k_{-2} \theta_{H_2O} \tag{4.21}$$

$$= \frac{k_2 K_1 \left(C_{H_2} - \frac{1}{K_e} C_{H_2O} \right)}{1 + K_1 C_{H_2} + K_3 C_{H_2O}} \tag{4.22}$$

and

$$k_r^{-1} = (k_2 K_1)^{-1} + k_2^{-1} C_{H_2} + k_2^{-1} (K_3/K_1) C_{H_2O} \tag{4.23}$$

If the solid state diffusion plays an important role in the reaction, equation 4.4a cannot be valid any more, and the step (4) has to be considered.

(d) solid state diffusion control

All step (1) to step (3) are in equilibrium and the excess metal ions occupy the surface sites. The equilibrium constant of step (2) becomes

$$K_2' = \frac{\theta_M \theta_{H_2O}}{\theta_{H_2}} \tag{4.24}$$

Then, the rate of diffusion is

$$R = R_4 = k_4 \theta_M \tag{4.25}$$

$$= k_4 K_2' \frac{\theta_{H_2}}{\theta_{H_2O}} \tag{4.26}$$

$$= k_4 \frac{K_1 K_2'}{K_3} \frac{C_{H_2}}{C_{H_2O}} \tag{4.27}$$

and

$$k_r^{-1} = k_4^{-1} \frac{K_3}{K_1 K_2'} C_{H_2O} \tag{4.28}$$

(e) both solid state diffusion and chemical process control

If the excess metal ions hinder the further reaction of oxide, the solid state diffusion can not be negligible any more. Some modifications have to be made in the derivation of the rate equation 4.21. The adsorbed hydrogen molecules are effective only on the surface with excess metal ions. The rate equation of step (2) then is

$$R_2 = k_2' \theta_{H_2/OM} - k_{-2}' \theta_{H_2O/M} \tag{4.29}$$

The equilibrium constants of adsorption and desorption becomes

$$K_1 = \frac{\theta_{H_2/OM}}{\theta_{S/OM} C_{H_2}} \tag{4.30}$$

$$K_3 = \frac{\theta_{H_2O/M}}{\theta_{S/M}\, C_{H_2O}} \tag{4.31}$$

If the concentration of adsorbates is very low, then

$$\theta_{S/OM} \simeq \theta_{OM} \tag{4.32}$$

and

$$\theta_{S/M} \simeq \theta_M \tag{4.33}$$

This assumption is always valid for physical adsorption at a temperature much higher than boiling point of adsorbate.

Balancing the overall surface sites, we obtain

$$\theta_M + \theta_{OM} = 1 \tag{4.34}$$

Under the assumption of steady state, the reaction rate must be the same for every steps.

$$R = R_2 = R_4 \tag{4.35}$$

Substituting $\theta_{H_2/OM}$, $\theta_{H_2O/M}$ of equation 4.30, 4.31, into equation 4.29

$$R_2 = k_2' K_1 \theta_{OM} C_{H_2} - k_{-2}' K_3 \theta_M C_{H_2O} \tag{4.36}$$

Combining equation 4.25, 4.34, 4.35, 4.36, we obtain the expression for θ_M

$$\theta_M = \frac{k_2' K_1 C_{H_2}}{k_4 + k_2' K_1 C_{H_2} + k_{-2}' K_3 C_{H_2O}} \tag{4.37}$$

The rate expression becomes

$$R = R_4 = k_4\theta_M \tag{4.38}$$

$$= \frac{k_4 k_2' K_1 C_{H_2}}{k_4 + k_2' K_1 C_{H_2} + k_{-2}' K_3 C_{H_2O}} \tag{4.39}$$

and

$$k_r^{-1} = k_2'^{-1} K_1^{-1} + k_4^{-1} C_{H_2} + k_4^{-1} \frac{K_3}{K_1 K_2'} C_{H_2O} \tag{4.40}$$

At this moment, the group K_1K_2'/K_3 does not represent the overall equilibrium constant K_e.

If the adsorption step were controlling, comparison of equation 4.14 with equation 3.1 would dictate that the water concentration, C_{H_2O}, would always equal the bulk hydrogen concentration, $C_{H_2}^b$. This conclusion is in conflict with the fact that there is no water in the beginning of the reaction.

If the desorption step were controlling, there should be no hydrogen concentration drop across the scale. The hydrogen concentration difference between the reaction interface and the bulk phase can be evaluated from the resistance of gas diffusion through the porous metal scale, as shown in Appendix 4, the difference is quite large.

If the chemical process step were controlling, the constants A_1 and A_2 in equation 3.1 would be:

$$A_1 = k_2^{-1} K_1^{-1} \tag{4.41}$$

$$A_2 = k_2^{-1} \tag{4.42}$$

and

$$C^b_{H_2} = C^i_{H_2} + K_3 K_1^{-1} C^i_{H_2O} \tag{4.43}$$

Then, A_2^{-1} would be the forward reaction rate constant of step (2) and $(A_1/A_2)^{-1}$ would be the adsorption equilibrium constant. Figure 9 shows the activation energies of A_1^{-1} and A_2^{-1} are 25 Kcal/mole and 10 Kcal/mole respectively. The heat of adsorption, which is the activation energy of adsorption equilibrium constant, is 15 Kcal/mole. However, the adsorption reaction is expected to be exothermal and the sign of the heat of adsorption is therefore expected to be negative. Thus, chemical process control alone cannot account for the experimental observations.

In the case of both solid state diffusion and chemical process control, the constant A_1^{-1} corresponds to k_2K_1 and A_2^{-1} corresponds to k_4. Their positive activation energies are quite plausible. The concentration requirement was obtained from the comparison of equation 3.1 with equation 4.40.

$$C^b_{H_2} = C^i_{H_2} + \frac{K_3}{K_1 K_2'} C^i_{H_2O} \tag{4.44}$$

The equilibrium constant group K_3/K_1K_2' will not vary in the experimental conditions. This means that the heat of adsorption of

water on the surface with excess metal ions equals the sum of the heat of adsorption of hydrogen on regular oxide surface sites plus the heat of reaction step (2), the overall heat of reaction is near zero.

The solid state diffusion step could involve both surface (interface) diffusion and volume diffusion. Consider a two dimensional periodic array of metal sinks with spacing λ, as shown in Fig. 8. The interface advancing rate, u, is related to the diffusivity and the spacing, λ. This is a problem analogous to that of cellular growth (16).

for volume diffusion

$$u \propto \frac{D_v}{\lambda} \tag{4.45}$$

for interface diffusion

$$u \propto \frac{D_s}{\lambda^2} \tag{4.46}$$

The interface reaction rate, R, is proportional to the interface advancing rate, u. This leads, for volume diffusion, to

$$k_4\lambda \propto D_v \tag{4.47}$$

and for interface diffusion to

$$k_4\lambda^2 \propto D_s \tag{4.48}$$

The SEM micrographs of the reaction interface in Fig. 10 give some ideas about the variation of spacing of metal precipitates

formed at 50 torr hydrogen between 460°C and 620°C. There is some tendency for λ to increase, but difference in this temperature range is not really measurable. Therefore, the activation energy of λ will not exceed +5 Kcal. The assessment of the importance of interface diffusion or volume diffusion in the experimental temperature range can be done by evaluating the activation energy of D_S or D_V. In the case of the volume diffusion activation energy for D_V could not exceed 15 Kcal/mole, which is too low for volume diffusion. In the case of interface diffusion, the activation energy for D_S would be about 20 Kcal/mole, which is quite plausible. It is therefore concluded that the interface reaction is controlled by an irreversible gas-oxide reaction at the pore base plus an interface diffusion of the generated excess cation to the metal phase.

5. SUMMARY

(1) The reduction reaction of cobalt ferrite by pure hydrogen in the temperature range of 560°C to 620°C and in the pressure range of 50 torr to 250 torr was under mixed control of the chemical reaction at the interface and of the gaseous diffusion through the metal scale.

(2) The gas diffusion through the metal scale was in the "transition" region. The effective diffusion coefficient was governed by the intergranular pore network at 560°C and by the intragranular pore network at 620°C.

(3) The interface reaction was shown to be controlled by both solid state diffusion and chemical process. The interface reaction rate can be expressed by an irreversible form of Langmuir-Hinshelwood kinetics. Interface diffusion of excess metal ions was the dominant mechanism in the solid state diffusion step.

ACKNOWLEDGMENTS

The author wishes to thank Professor Lutgard C. De Jonghe for his continuous guidance and encouragement in this research work.

This work was supported by the Division of Material Science, Office of Basic Energy Science, U.S. Department of Energy, under contract no. W-7405-ENG-48.

REFERENCES

1. N. E. Ranz, W. R. Marshall, Jr., Chem. Eng. Prog. 48, 141 (1952)
2. A. W. D. Hills, Met. Trans. 9B, 121 (1978)
3. W. M. McKewan, Steelmaking: The Chipman Conference, 141 (1962)
4. R. H. Spitzer, F. S. Manning, W. O. Philbrook, Trans. Met. Soc. AIME, 236, 726 (1966)
5. E. T. Turkdogan, J. V. Vinters, Met. Trans., 2, 3175 (1971)
6. E. T. Turkdogan, R. G. Olsson, J. V. Vinters, Met. Trans., 2, 3189 (1971)
7. E. T. Turkodgan, J. V. Vinters, Met. Trans., 3, 1561 (1972)
8. R. H. Tien, E. T. Turkdogan, Met. Trans., 3, 2039 (1972)
9. J. Szekeley, J. W. Evans, H. Y. Sohn, "Gas-Solid Reaction" Academic Press. N.Y. (1976)
10. J. R. Porter, L. C. De Jonghe, LBL Report No. 9801
11. M. C. Rey, Ph.D. Thesis, Cornell University (1979)
12. C. Wagner, Steelmaking: The Chipman Conference, 19 (1962)
13. C. N. Satterfield, "Mass Transfer in Heterogeneous Catalysis" MIT Press, (1968)
14. G. R. Youngquist, I & EC, 62, 8, 52 (1970)
15. N. Wakao, J. M. Smith, Chem. Eng. Sci. 17, 825 (1962)
16. M. E. Fine, "Introduction to Phase Transformations in Condensed Systems", McMillan Co. N.Y., p. 86 (1965)
17. R. B. Bird, W. E. Stewart, E. N. Lightfoot, "Transport Phenomena" Wiley, (1960)

Table 1. Effective Diffusion Coefficient, D_{eff} (cm^2/sec)

Temperature (°C)	Pressure (torr)				
	50	100	150	200	250
560	0.13	0.12	0.11	0.14	0.13
580	0.15	0.14	0.11	0.11	0.11
600	0.13	0.15	0.13	0.11	0.189
620	0.076	0.073	0.080	0.098	0.087

Table 2. The Value of $(k_m^{-1} + k_r^{-1})^{-1}$ (cm/sec)

Temperature (°C)	Pressure (torr)				
	50	100	150	200	250
560	6.09	4.30	3.66	3.24	2.72
580	7.22	5.80	4.67	3.63	3.23
600	10.4	7.43	5.94	4.83	4.25
620	12.6	11.9	7.36	6.09	4.95

FIGURE CAPTIONS

Figure 1. Schematic diagram of the shrinking core model for a gas solid reaction. (XBL 805-5237)

Figure 2. Schematic diagram of the thermogravimetric analysis apparatus. (XBL 794-9305)

Figure 3. Reduction kinetics in 200 torr hydrogen. Calculated layer thickness versus time. (XBL 805-5232)

Figure 4. Reduction kinetics at 580°C. Calculated layer thickness versus time. (XBL 805-5233)

Figure 5. Reduction kinetics at 580°C. Reciprocal interface advance rate versus layer thickness. (XBL 805-5234)

Figure 6. The reciprocal interface reaction rate constant as a function of bulk hydrogen pressure, showing that the rate follows Langmuir-Hinshelwood kinetics. (XBL 805-5235)

Figure 7. SEM micrographs of metal scale: (a) at 560°C in 50 torr hydrogen for 300 seconds. (b) at 560°C in 250 torr hydrogen for 150 seconds. (c) at 620°C in 250 torr hydrogen for 120 seconds. (d) (e) at 620°C in 50 torr hydrogen for 240 seconds, showing the macropore network and micropore network. (XBB 806-6910; XBB 806-6909)

Figure 8. Schematic diagram of the interface reaction, with the spacing between the metal = λ. (XBL 796-10416)

Figure 9. Arrhenius plot for the rate constant A_1^{-1} and A_2^{-1} of the equation 3.1. The activation energy of A_1^{-1} is 25 Kcal/mole and that of A_2^{-1} is 10 Kcal/mole. (XBL 805-5236)

Figure 10. SEM micrographs of reaction interface: (a) at 560°C in 50 torr hydrogen for 200 seconds. (b) at 620°C in 50 torr hydrogen for 450 seconds, showing the spacing between the interface metal precipitates.

(XBB 806-6908)

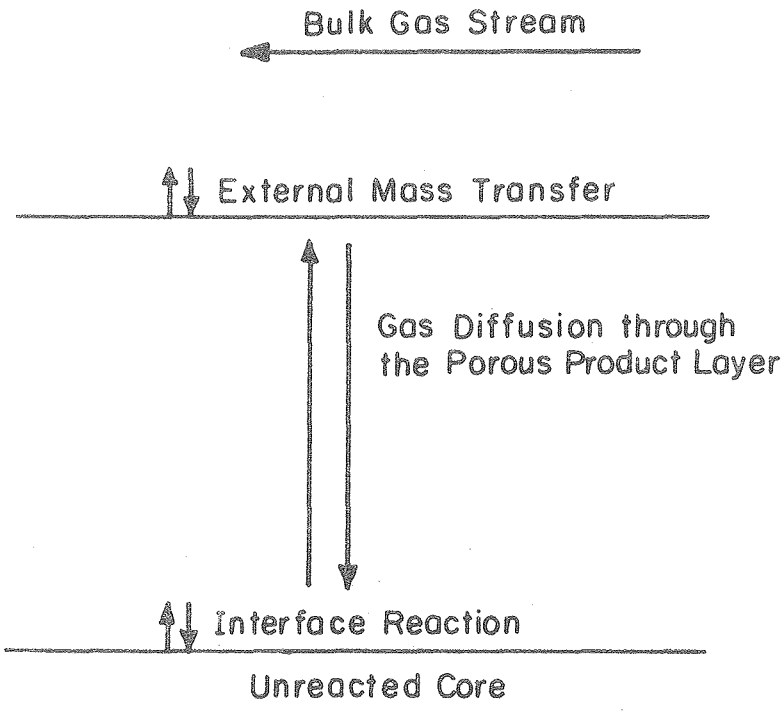
Bulk Gas Stream
External Mass Transfer
Gas Diffusion through
the Porous Product Layer
Interface Reaction
Unreacted Core
XBL805-5237

Figure 1

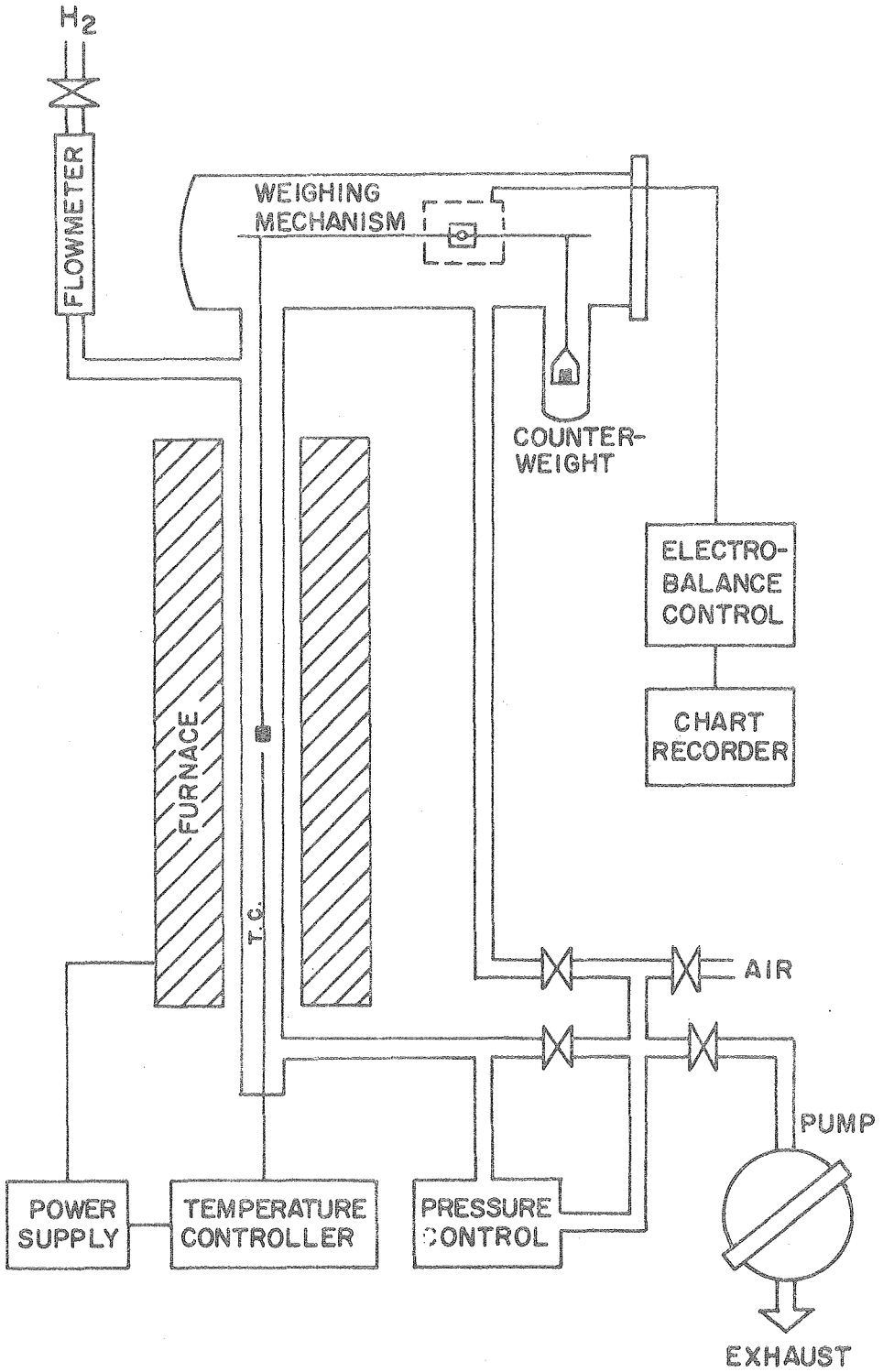

XBL 794-9305

Figure 2

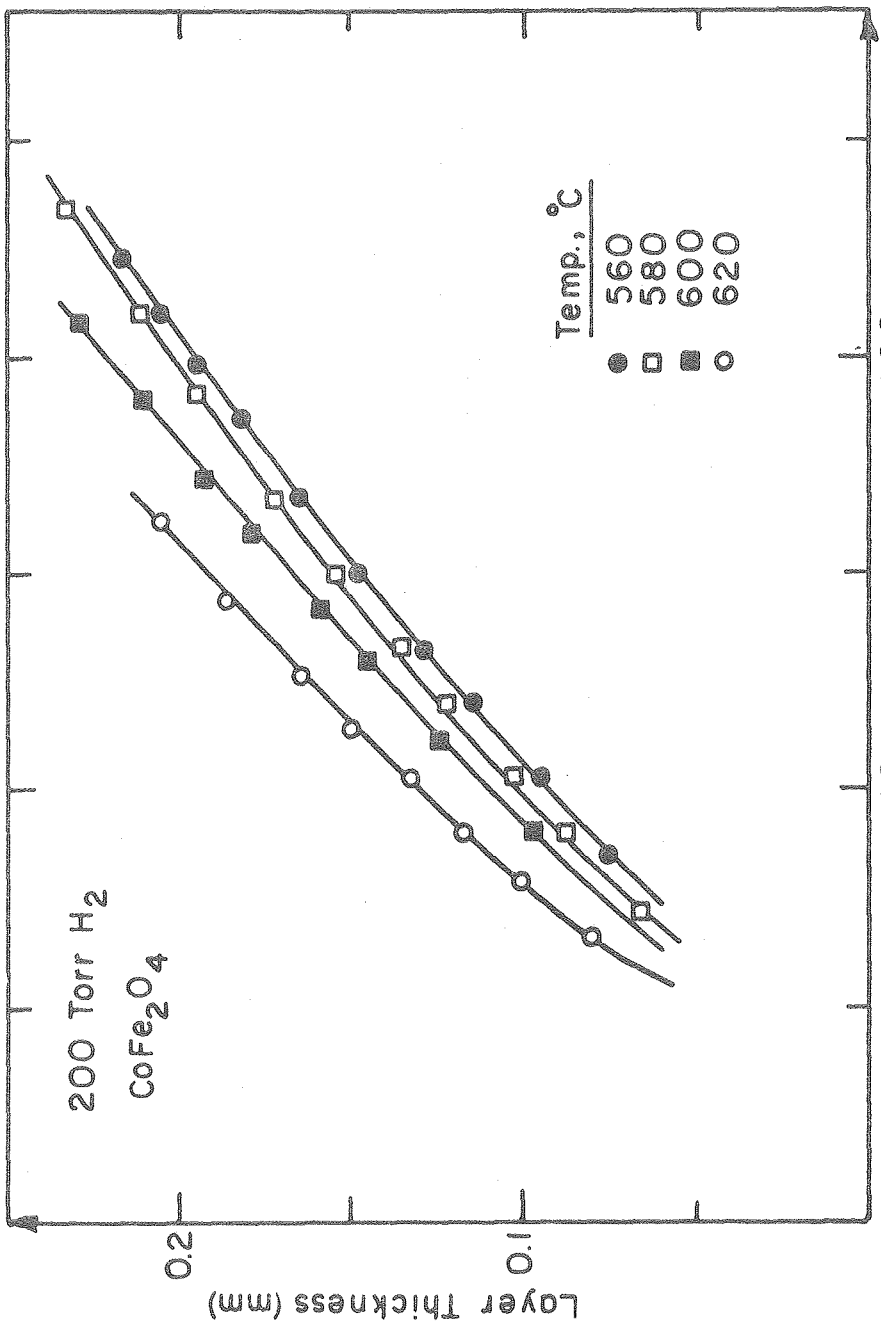

XBL 805-5232

Figure 3

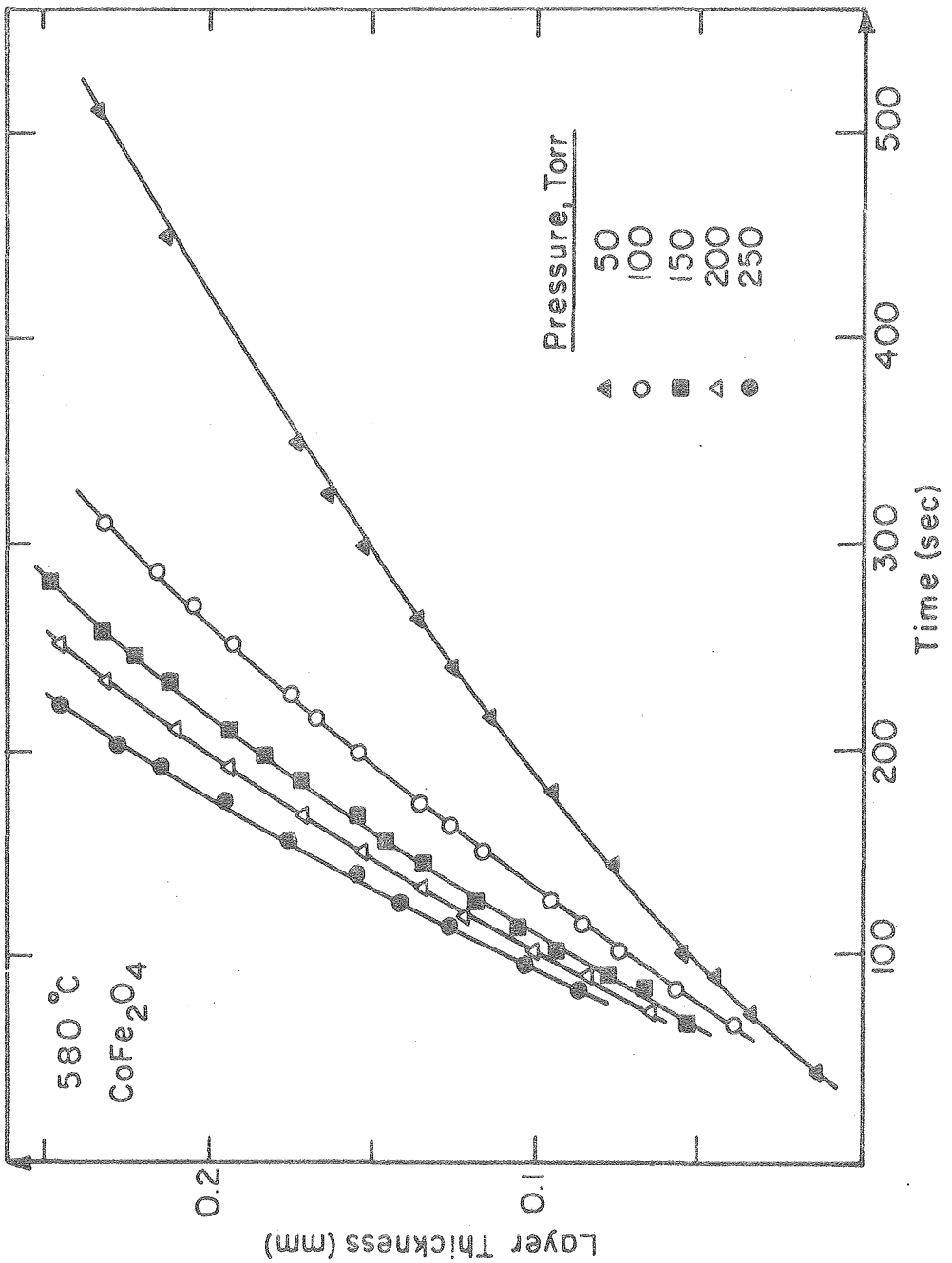

XBL 805-5233

Figure 4

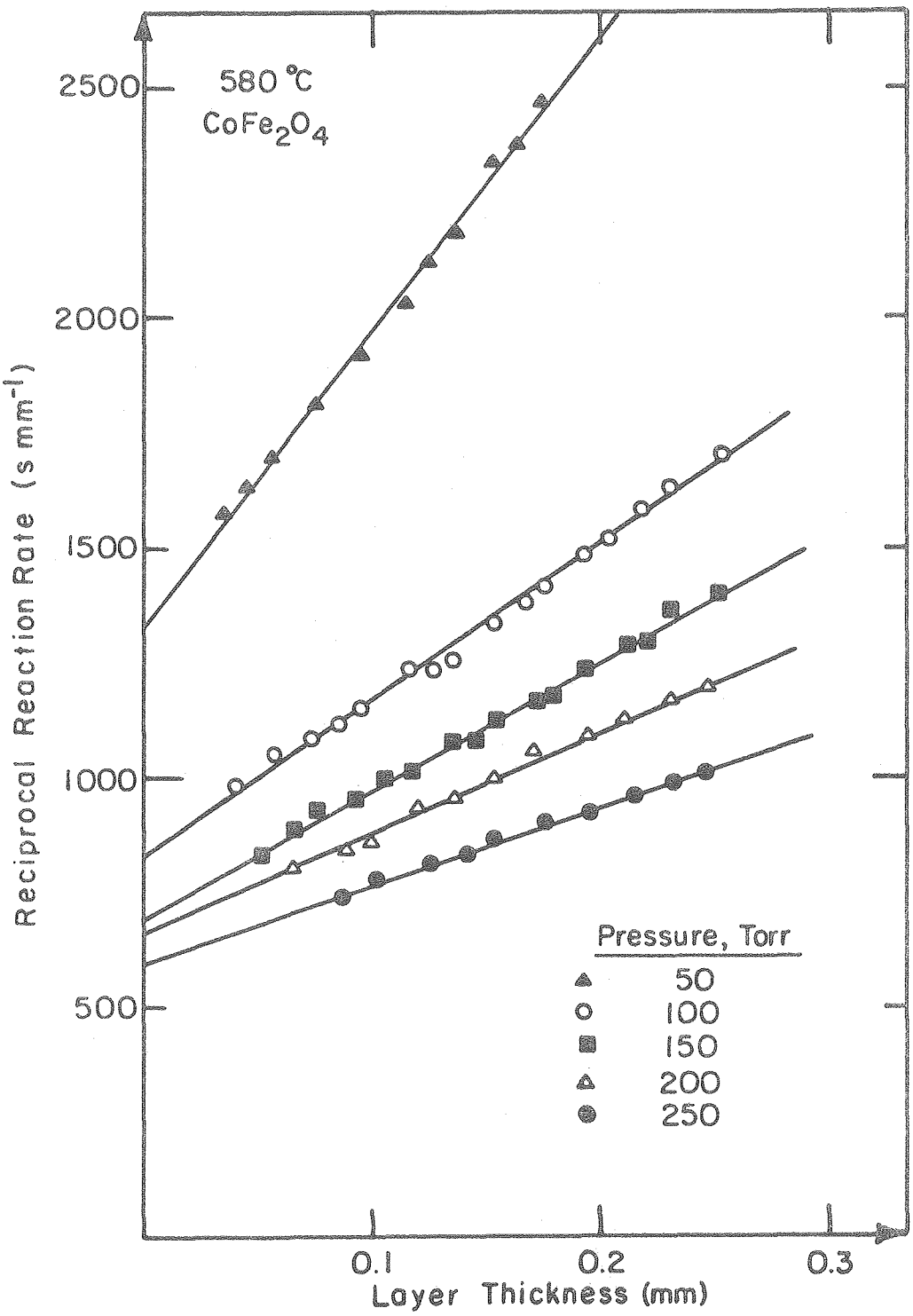
580 °C
$CoFe_2O_4$
2500
2000
1500
1000
500
Reciprocal Reaction Rate (s mm^{-1})
Pressure, Torr
50
100
150
200
250
0.1
0.2
0.3
Layer Thickness (mm)
XBL 805-5234

Figure 5

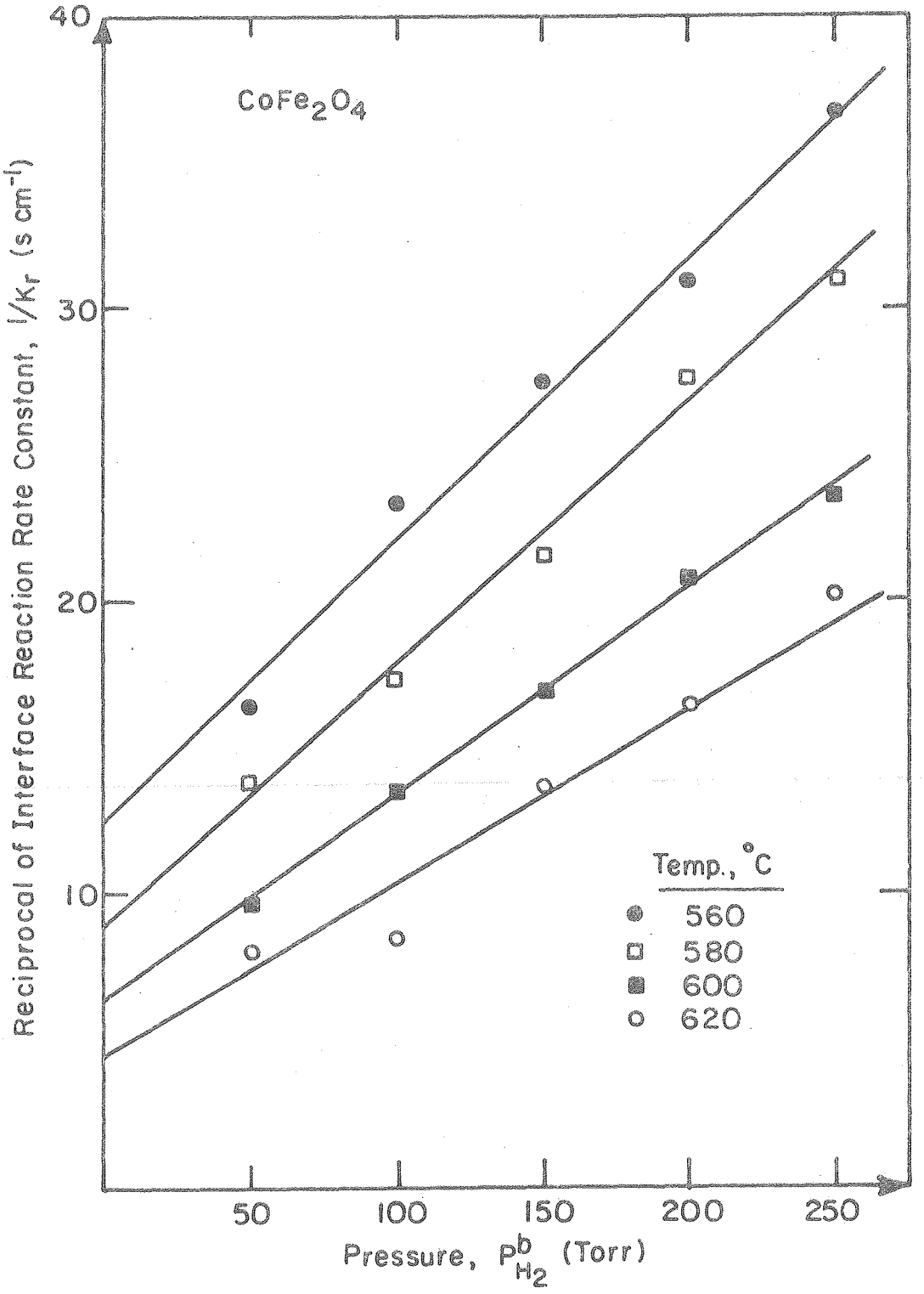
40
30
20
10
$CoFe_2O_4$
Reciprocal of Interface Reaction Rate Constant, $1/K_r$ (s cm^{-1})
Temp., °C
560
580
600
620
50
100
150
200
250
Pressure, $P^b_{H_2}$ (Torr)
XBL805-5235

Figure 6

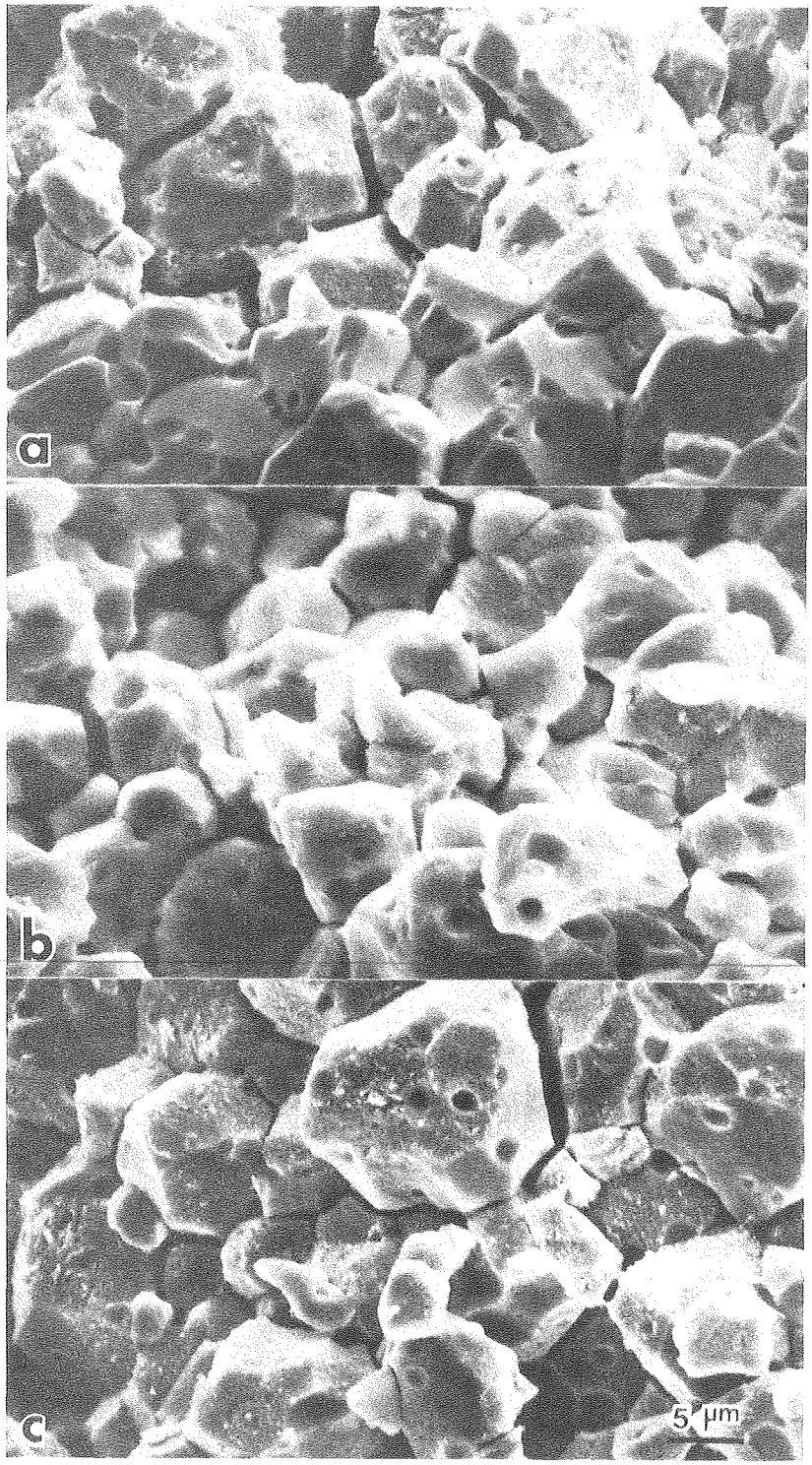

XBB 806-6910

Figure 7

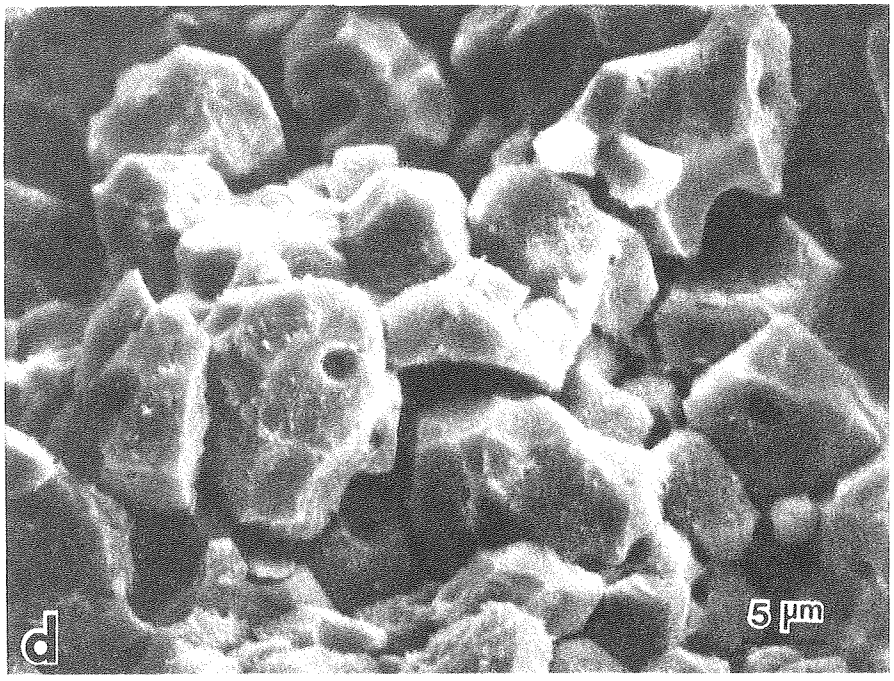

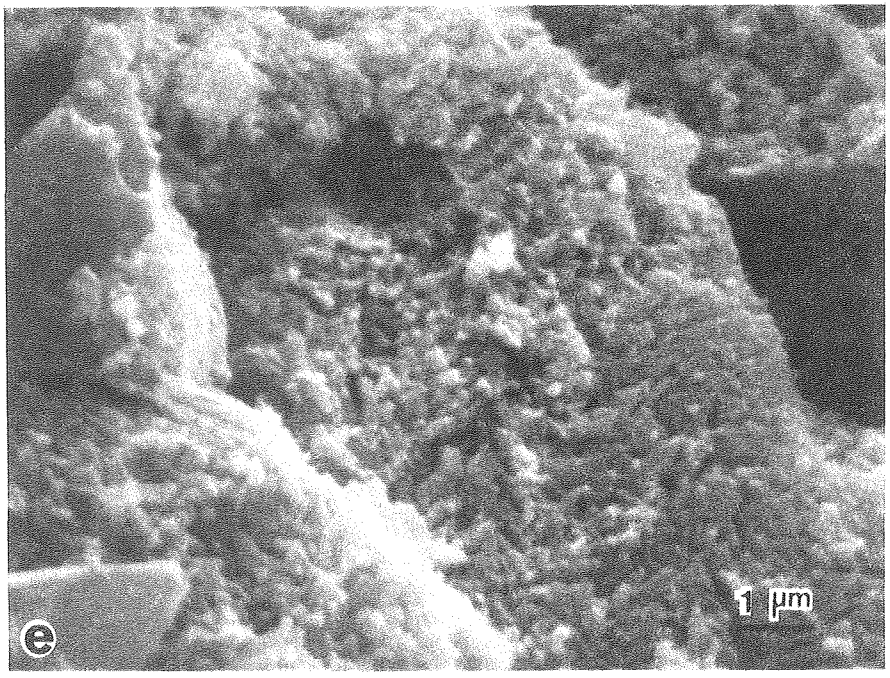

XBB 806-6909

Figure 7 (continued)

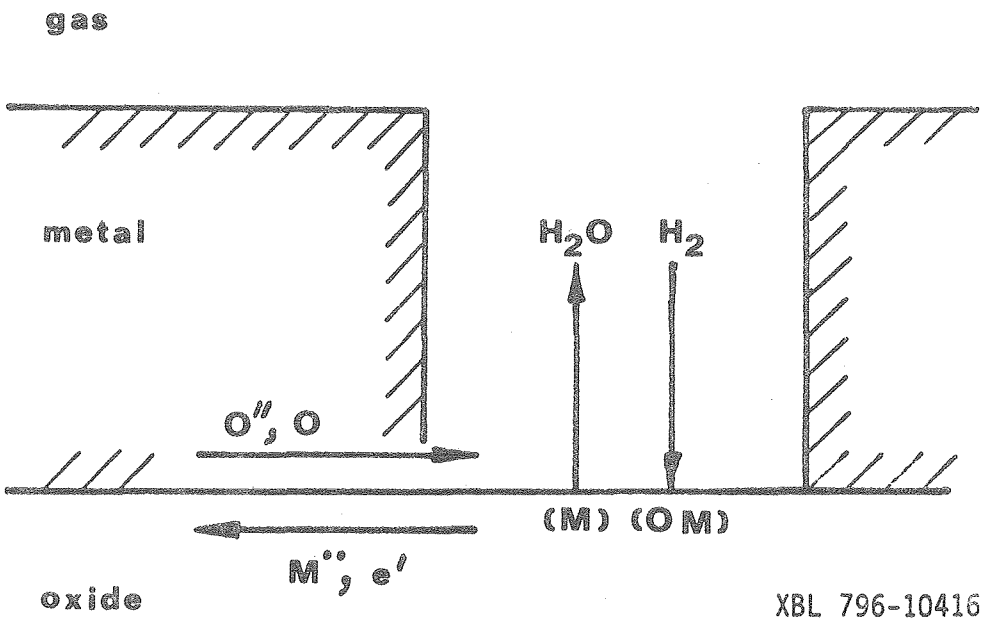

Figure 8

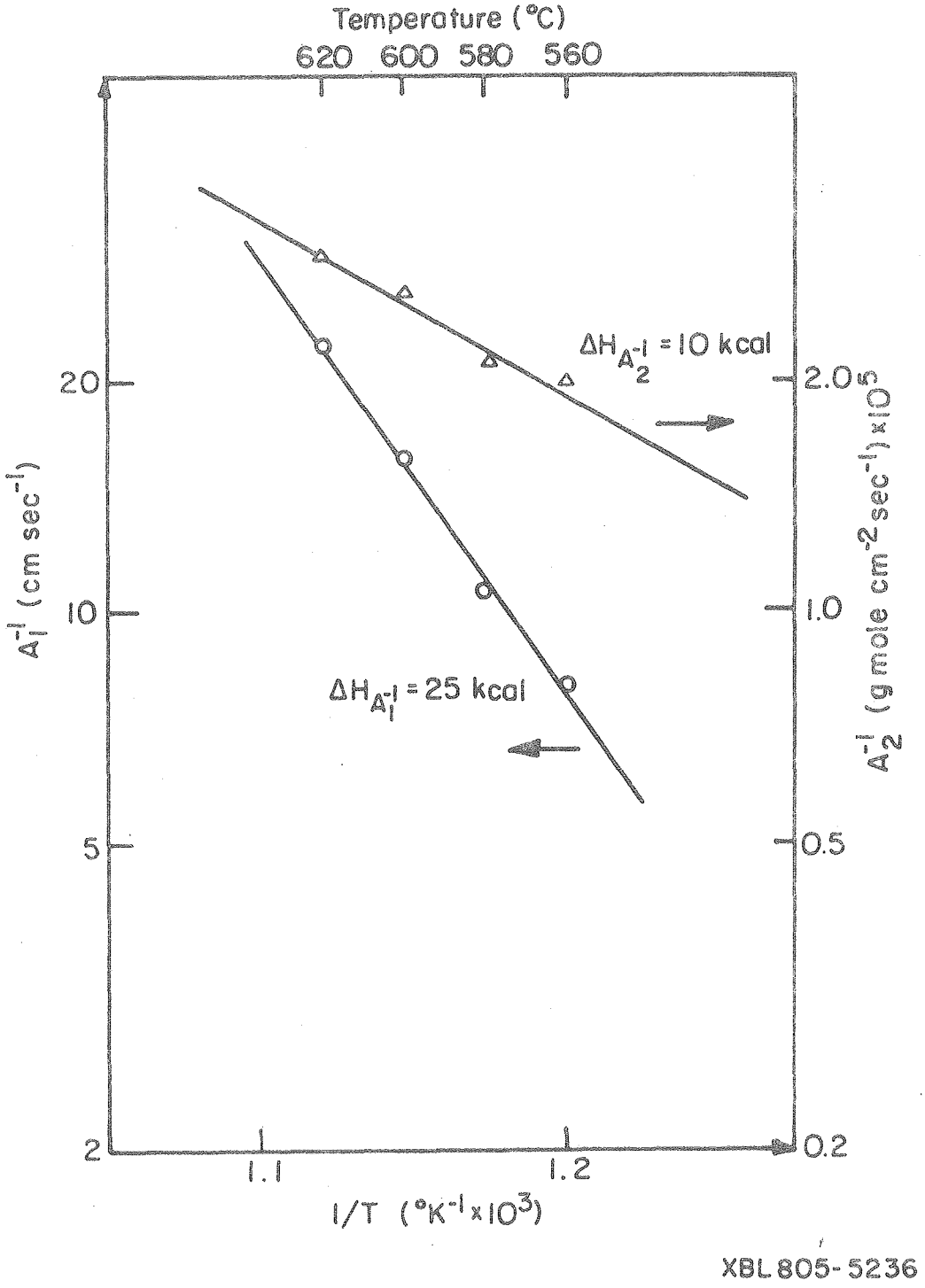
Temperature (°C)
620 600 580 560
$\Delta H_{A_2^{-1}}$ = 10 kcal
$\Delta H_{A_1^{-1}}$ = 25 kcal
A_1^{-1} (cm sec^{-1})
A_2^{-1} (g mole cm^{-2} sec^{-1}) x10^5
20
10
5
2
2.0
1.0
0.5
0.2
1.1
1.2
1/T (°K^{-1} x10^3)
XBL 805-5236

Figure 9

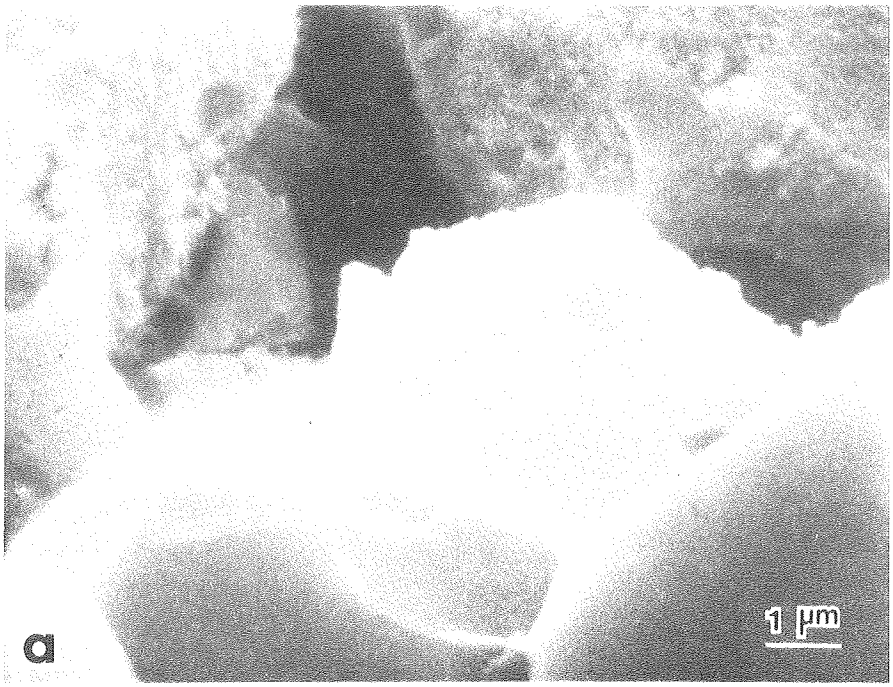

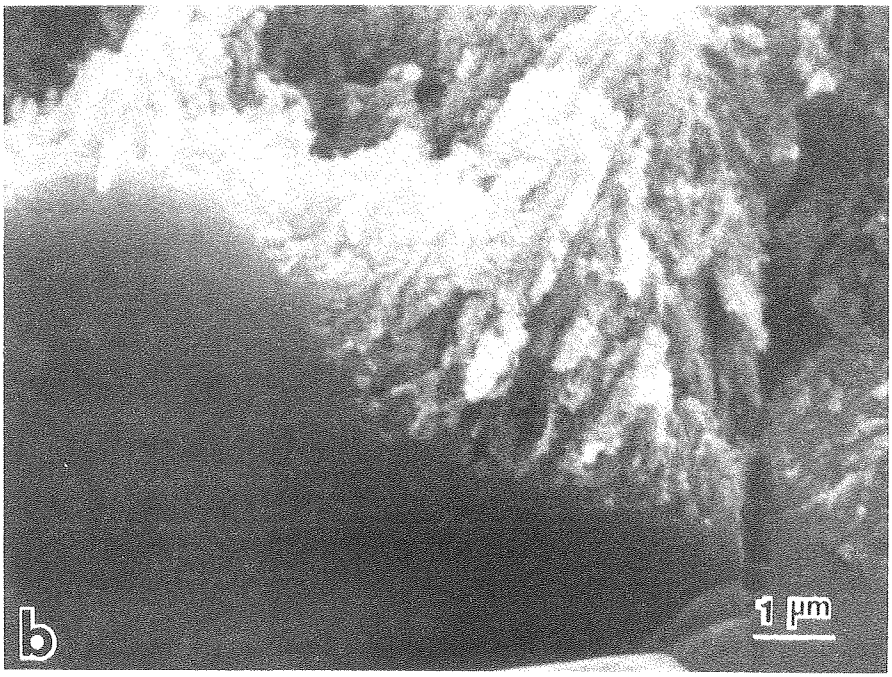

XBB 806-6908

Figure 10

APPENDIX 1

External Mass Transfer Coefficient, k_m

According to the equation of Ranz and Marshall

$$N_{Sh} = 2.0 + 0.6\, N_{Re}^{1/2} N_{Sc}^{1/3} \qquad (A1.1)$$

The external mass transfer coefficient is calculated from a knowledge of Sherwood number which is a function of Reynolds number and Schmidt number.

$$\text{Sherwood number, } N_{Sh} = \frac{k_m L}{D} \qquad (A1.2)$$

$$\text{Reynolds number, } N_{Re} = \frac{\rho V L}{\mu} \qquad (A1.3)$$

$$\text{Schmidt number, } N_{Sc} = \frac{\mu}{\rho D} \qquad (A1.4)$$

The binary diffusion coefficient, D, can be estimated from the Chipman-Enskog equation:

$$D_{H_2/H_2O} = \frac{1.8583 \times 10^{-3} \sqrt{T^3 \left(\frac{1}{M_{H_2}} + \frac{1}{M_{H_2O}}\right)}}{p\sigma^2\Omega} \qquad (A1.5)$$

and the gas viscosity can be estimated from a similar equation:

$$\mu = 2.6693 \frac{\sqrt{MT}}{\sigma^2 \Omega_\mu} \qquad (A1.6)$$

The values of Ω and σ can be found in the book of Bird et al. (17).

At 600°C and 50 torr, the parameters are

$$L = 0.6 \text{ cm}$$

$$V = 178 \text{ cm/sec}$$

$$D = 82.09 \text{ cm}^2/\text{sec}$$

$$\mu_{H_2} = 1.77 \times 10^{-4} \text{ Poise}$$

$$\rho_{H_2} = 9.18 \times 10^{-7} \text{ g/cm}^3$$

Substituting these values into equation A1.1, the value of external mass transfer coefficient can be obtained

$$k_m = 378 \text{ cm/sec}$$

similarly, at 600°C and 250 torr

$$k_m = 75 \text{ cm/sec}$$

The values of k_m in the same pressure do not vary much in the temperature range of 560°C to 620°C.

APPENDIX 2

Gas Diffusion Coefficient in Porous Media

(1) ordinary molecular diffusion coefficient for binary system of H_2/H_2O

D_{H_2/H_2O} was estimated from the equation A1.5

D_{H_2/H_2O} (cm^2/sec)	50 torr	250 torr
560°C	75.7	15.1
620°C	85.4	17.1

(2) Knudsen diffusion coefficient

For cylindrical pores with radius r, the Knudsen diffusion coefficient is

$$D_K = \frac{2}{3} r \left(\frac{8R_g T}{\pi M}\right)^{1/2} \qquad \text{(A2.1)}$$

The size of the pores were in the range of 0.2 μ to 2.0 μ. Then, the Knudsen diffusion coefficient of hydrogen is

D_{KH_2} (cm^2/sec)	0.2 μ	2.0 μ
560°C	3.96	39.6
620°C	4.10	41.0

APPENDIX 3

Effective Gas Diffusion Coefficient

(1) estimation of effective gas diffusion coefficient by equation 4.2

$$D_{eff} = \left[\varepsilon_a^2 D_a + \varepsilon_i^2 D_i + 2\varepsilon_a(1-\varepsilon_a) \left(\frac{2\varepsilon_i^2}{\frac{\varepsilon_i^2}{D_a} + \frac{(1-\varepsilon_a)^2}{D_i}} \right) \right]$$

where

$$D_a = \frac{1}{\frac{1}{D_{Ka}} + \frac{1}{D_{H_2/H_2O}}}$$

$$D_i = \frac{1}{\frac{1}{D_{Ki}} + \frac{1}{D_{H_2/H_2O}}}$$

Values of parameters:

Temperature (^oC)	Pressure (torr)	
	50	250
	r_a = 1.7 μ	2
	r_i = 0.025 μ	0.02
	ε_a = 0.1	0.06
	ε_i = 0.4	0.44
560	D_{H_2/H_2O} = 76 cm^2/sec	15
	D_{Ka} = 34 cm^2/sec	40
	D_{Ki} = 0.50 cm^2/sec	0.4
	D_a = 23.5 cm^2/sec	11
	D_i = 0.50 cm^2/sec	0.39
	D_{eff} = 0.31 cm^2/sec	0.11

Temperature (°C)	Pressure (torr)	
	50	250
	r_a = 0.25 μ	0.2
	r_i = 0.045 μ	0.04
	ε_a = 0.04	0.01
	ε_i = 0.46	0.49
620	D_{H_2/H_2O} = 85 cm^2/sec	17
	D_{Ka} = 4.9 cm^2/sec	4.0
	D_{Ki} = 0.89 cm^2/sec	0.79
	D_a = 4.6 cm^2/sec	3.2
	D_i = 0.87 cm^2/sec	0.39
	D_{eff} = 0.18 cm^2/sec	0.097

(2) comparison of calculated and measured values of D_{eff} (cm^2/sec)

Temperature (°C)	Pressure (torr)	
	50	250
560	$D_{eff\ calc.}$ = 0.31	0.11
	$D_{eff\ meas.}$ = 0.13	0.13
620	$D_{eff\ calc.}$ = 0.18	0.097
	$D_{eff\ meas.}$ = 0.076	0.087

APPENDIX 4

Gas Concentration at the Reaction Interface

Considering the scale resistance only, the concentration at the reaction interface is

$$C^i_{H_2} = C^b_{H_2} - \frac{J}{D_{effH_2}} \tag{A4.1}$$

$$C^i_{H_2O} = C^b_{H_2O} + D\frac{J}{_{effH_2O}} \tag{A4.2}$$

(1) at 620°C and 250 torr

$$C^b_{H_2} = 4.50 \times 10^{-6} \text{ gmole/cm}^3$$

$$D_{effH_2} = 0.09 \text{ cm}^2/\text{sec}$$

at $\xi = 0.2$ mm

$$J = 1.08 \times 10^{-5} \text{ gmole/sec cm}^2$$

Then, the hydrogen concentration is obtained

$$C^i_{H_2} = 2.1 \times 10^{-6} \text{ gmole/cm}^3$$

assuming

$$D_{effH_2O} \cong \frac{1}{3} \; D_{effH_2}$$

we obtain

$$C^{i}_{H_2O} = 7.2 \times 10^{-6} \text{ gmole/cm}^3$$

(2) at 620°C and 50 torr

$$C^{b}_{H_2} = 0.90 \times 10^{-6} \text{ gmole/cm}^3$$

Similarly, we obtain

at $\xi = 0.15$ mm

$$C^{i}_{H_2} = 3.0 \times 10^{-7} \text{ gmole/cm}^3$$

$$C^{i}_{H_2O} = 1.8 \times 10^{-6} \text{ gmole/cm}^3$$

(3) at 560°C and 250 torr

$$C^{b}_{H_2} = 4.72 \times 10^{-6} \text{ gmole/cm}^3$$

at $\xi = 0.2$ mm

$$C^{i}_{H_2O} = 4.7 \times 10^{-6} \text{ gmole/cm}^3$$

$$C^{i}_{H_2O} = 4.7 \times 10^{-7} \text{ gmole/cm}^3$$

(4) at 560°C and 50 torr

$$C^{b}_{H_2} = 0.94 \times 10^{-6} \text{ gmole/cm}^3$$

at $\xi = 0.2$ mm

$$C^{i}_{H_2} = 4.9 \times 10^{-7} \text{ gmole/cm}^3$$

$$C^{i}_{H_2O} = 1.4 \times 10^{-6} \text{ gmole/cm}^3$$